

UMass Chan Medical School

eScholarship@UMassChan

---

Open Access Publications by UMMS Authors

---

2021-04-12

## Therapeutic B-cell depletion reverses progression of Alzheimer's disease

Ki Kim

*National Institute on Aging*

*Et al.*

Let us know how access to this document benefits you.

Follow this and additional works at: <https://escholarship.umassmed.edu/oapubs>



Part of the Immunology and Infectious Disease Commons, Nervous System Diseases Commons, Neurology Commons, Neuroscience and Neurobiology Commons, Psychiatry and Psychology Commons, and the Translational Medical Research Commons

---

### Repository Citation

Kim K, Wang X, Ragonnaud E, Bodogai M, Illouz T, DeLuca M, McDevitt RA, Gusev F, Okun E, Rogaeve EI, Biragyn A. (2021). Therapeutic B-cell depletion reverses progression of Alzheimer's disease. Open Access Publications by UMMS Authors. <https://doi.org/10.1038/s41467-021-22479-4>. Retrieved from <https://escholarship.umassmed.edu/oapubs/4698>






Creative Commons License



This work is licensed under a [Creative Commons Attribution 4.0 License](https://creativecommons.org/licenses/by/4.0/).

This material is brought to you by eScholarship@UMassChan. It has been accepted for inclusion in Open Access Publications by UMMS Authors by an authorized administrator of eScholarship@UMassChan. For more information, please contact [Lisa.Palmer@umassmed.edu](mailto:Lisa.Palmer@umassmed.edu).

# Therapeutic B-cell depletion reverses progression of Alzheimer's disease

Ki Kim <sup>1,10</sup>, Xin Wang<sup>1,10</sup>, Emeline Ragonnaud<sup>1,10</sup>, Monica Bodogai<sup>1,10</sup>, Tomer Illouz <sup>2,3,4</sup>, Marisa DeLuca <sup>1</sup>, Ross A. McDevitt<sup>5</sup>, Fedor Gusev<sup>6</sup>, Eitan Okun <sup>2,3,4</sup>, Evgeny RogaeV<sup>6,7,8,9</sup> & Arya Biragyn <sup>1</sup>✉

The function of B cells in Alzheimer's disease (AD) is not fully understood. While immunoglobulins that target amyloid beta (A $\beta$ ) may interfere with plaque formation and hence progression of the disease, B cells may contribute beyond merely producing immunoglobulins. Here we show that AD is associated with accumulation of activated B cells in circulation, and with infiltration of B cells into the brain parenchyma, resulting in immunoglobulin deposits around A $\beta$  plaques. Using three different murine transgenic models, we provide counterintuitive evidence that the AD progression requires B cells. Despite expression of the AD-fostering transgenes, the loss of B cells alone is sufficient to reduce A $\beta$  plaque burden and disease-associated microglia. It reverses behavioral and memory deficits and restores TGF $\beta$ <sup>+</sup> microglia, respectively. Moreover, therapeutic depletion of B cells at the onset of the disease retards AD progression in mice, suggesting that targeting B cells may also benefit AD patients.

<sup>1</sup>Immunoregulation Section, Laboratory of Immunology and Molecular Biology, National Institute on Aging, Baltimore, MD, USA. <sup>2</sup>The Mina and Everard Goodman faculty of Life Sciences, Ramat Gan, Israel. <sup>3</sup>The Gonda Brain Research Center, Bar Ilan University, Ramat Gan, Israel. <sup>4</sup>The Paul Feder Laboratory on Alzheimer's disease research, Bar Ilan University, Ramat Gan, Israel. <sup>5</sup>Mouse Phenotyping Unit, Comparative Medicine Section, National Institute on Aging, Baltimore, MD, USA. <sup>6</sup>Department of Genomics and Human Genetics, Institute of General Genetics, Russian Academy of Sciences, Moscow, Russia. <sup>7</sup>Center for Genetics and Genetic Technologies, Faculty of Biology, Faculty of Bioengineering and Bioinformatics, Lomonosov Moscow State University, Moscow, Russia. <sup>8</sup>Department of Psychiatry, University of Massachusetts Medical School, Worcester, MA, USA. <sup>9</sup>Sirius University of Science and Technology, Sochi, Russia. <sup>10</sup>These authors contributed equally: Ki Kim, Xin Wang, Emeline Ragonnaud, Monica Bodogai. ✉email: [biragyna@mail.nih.gov](mailto:biragyna@mail.nih.gov)

**A**lzheimer's disease (AD) is a progressive neurodegenerative disease that mostly affects elderly people. It is associated with impaired clearance of toxic protein aggregates from the brain parenchyma, such as amyloid- $\beta$  (A $\beta$ ) peptides of aberrantly cleaved amyloid precursor protein (APP)<sup>1</sup>. Although resident microglial cells phagocytize extracellular A $\beta$  plaques with the help of astrocytes and TGF $\beta$  (refs. 2,3), chronic inflammation, and A $\beta$  production dysregulate this process, causing proliferation and subsequent replacement of homeostatic microglia with disease-associated microglia (DAM)<sup>4</sup>. As in mice with genetic TGF $\beta$  deficiency, which suffer from microgliosis and neuronal death<sup>5</sup>, DAM further exacerbate neuroinflammation and neuronal degeneration in AD<sup>6,7</sup>, at least in part, through expression of proinflammatory cytokines and downregulation of phagocytosis of A $\beta$  plaques<sup>8–10</sup>. Consistent with a positive association between AD risk and old age<sup>11</sup>, when systemic inflammation is increased<sup>12</sup>, disease progression also depends on peripheral inflammation and activation of innate immune cells<sup>13</sup>. The role of the adaptive immunity in AD however remains poorly understood, and is mostly linked to T cells exerting both beneficial and harmful functions. For example, in APP/PS1 mice expressing the K670N and M671L Swedish mutations of human APP and L166P mutated presenilin 1 (PS1), the infiltration of Th1 CD4<sup>+</sup> T cells in the brain either improves<sup>14</sup> or exacerbates AD<sup>15</sup>. Moreover, the amelioration of AD in Rag2-deficient APP/PS1 mice is primarily linked to the loss of pathogenic T cells<sup>16</sup>. Although Rag deficiency also retards development of functional B cells (besides T cells), the role of B cells in AD is rarely explored and mostly considered to be beneficial. Their main product, nonspecific immunoglobulin and A $\beta$ -specific antibodies in peripheral blood (PB) and cerebrospinal fluid (CSF) of people<sup>17,18</sup> and mice<sup>19,20</sup> with AD, provides neuroprotective benefit. In 5 $\times$ FAD mice, which overexpress APP with the Swedish (K670N, M671L), Florida (I716V) and London (V717I) mutations, and PS1 with M146L and L286V mutations, Rag deficiency exacerbates AD due to loss of nonspecific immunoglobulin that activates microglial phagocytosis and consequent clearance of A $\beta$  plaques<sup>21</sup>. However, B cells are a heterogeneous population of cells. Their function and subset accumulation are regulated by the inflammatory milieu. For example, we recently reported that inflammaging activates monocytes to convert innate B1a cells into pathogenic 4-1BBL<sup>+</sup> TNF $\alpha$ <sup>+</sup> MHC-I<sup>High</sup> B cells (termed 4BL cells), which then induce cytolytic CD8<sup>+</sup> T cells and insulin resistance in elderly humans, macaques, and mice<sup>22,23</sup>. However, the role of these or other activated B cells in aging-associated diseases, such as AD remains unknown.

Here, using three, widely utilized transgenic AD mouse models with or without genetic B-cell deficiency, we provide evidence and mechanistic insight that the loss of mature B cells alone is sufficient to markedly retard the AD progression. Although B cells are thought not to infiltrate the AD brain, we link their presence in the brain parenchyma to the disease progression. Importantly, therapeutic depletion of circulating B cells at the onset of the disease eliminates B cells, and their immunoglobulin deposits in the brain and blocks the AD manifestation. Our data not only warrants a new look to B cells as pathogenic, AD-promoting cells in humans with AD, but also suggests that their B cells should be targeted to control the disease progression.

## Results

To assess the involvement of B cells in AD, we first performed a flow cytometry evaluation of B cells in the circulation of congenic and sex- and age-matched C57BL/6 (WT) and 3 $\times$ TgAD mice, a model for early-onset AD (EOAD, harbors the Swedish APP mutation, the M146V mutation on PS1 and the P301L in MAPT)<sup>24,25</sup>. Note: from here on and unless specified, we used

aged (60–70 weeks old) female 3 $\times$ TgAD mice due to their more pronounced AD-like symptom manifestation<sup>25</sup>. Compared with control mice, 3 $\times$ TgAD mice significantly upregulated the frequency and numbers of B cells in the circulation and secondary lymphoid organs (Supplementary Fig. 1A and not depicted; gating strategy is in Supplementary Fig. 9A), with innate CD5<sup>+</sup> B1a and CD5<sup>−</sup> B1b cells (CD11b<sup>+</sup> or/and CD23<sup>−</sup> CD43<sup>+</sup> CD19<sup>+</sup> cells, respectively) markedly increased, and conventional B2 cells decreased in the spleen and cervical lymph nodes (cLN; Fig. 1A–C and Supplementary Fig. 1B–D). The 3 $\times$ TgAD mice also contained higher amounts of activated B cells expressing IFN $\gamma$ , IL6, IL10, and TGF $\beta$  in circulation than control mice (Fig. 1D–G), mostly within B1a cells and, at lesser extent B1b and follicular B cells (Supplementary Fig. 1E–H). The AD mouse B cells, particularly B1a cells, markedly upregulated 4-1BBL (Supplementary Fig. 1I, J), resembling pathogenic B1a cells of aged subjects<sup>22,23</sup> and suggesting their potential involvement in AD. To test this possibility, we have generated B-cell-deficient 3 $\times$ TgAD mice (termed 3 $\times$ TgAD-BKO, Supplementary Fig. 2A) by crossing 3 $\times$ TgAD mice with J<sub>H</sub>T mice, which lack functional B cells due to the immunoglobulin J<sub>H</sub> locus deletion that terminates B-cell development at the pro-B cell stage<sup>26</sup>. When mice reached 50–60 weeks of age, they were evaluated for hippocampus-dependent cognitive behavior, using the Morris water maze (MWM) task. During the 5-day hidden platform training, both 3 $\times$ TgAD and 3 $\times$ TgAD-BKO mice showed comparable performance (not depicted). However, 24 h after the last training session, a probe trial conducted in the absence of the hidden platform, revealed that 3 $\times$ TgAD-BKO mice spent a significantly longer time in the target quadrant than their 3 $\times$ TgAD littermates ( $p = 0.017$ ,  $n = 13–15$ , Fig. 2A), indicating a stronger spatial memory of the platform's location. We also tested exploratory behavior anomalies using the open field arena (OFA, a commonly used assay in 3 $\times$ TgAD mice<sup>27,28</sup>). While 3 $\times$ TgAD mice exhibited reduced activity as compared with WT mice in the OFA, the impairment was no longer detectable in age-matched 3 $\times$ TgAD-BKO littermates (left panel, one-way ANOVA  $F(2,29) = 21.68$ ,  $p < 0.0001$ ; WT vs 3 $\times$ TgAD  $p < 0.0001$ , 3 $\times$ TgAD vs 3 $\times$ TgAD-BKO  $p < 0.0001$ ,  $n = 10–11$ , and Fig. 2B), implying that 3 $\times$ TgAD-associated behavioral impairments required B cells.

To confirm this conclusion, we tested APP/PS1 mice, another model of EOAD, that exhibit earlier AD pathology compared with 3 $\times$ TgAD mice<sup>29</sup>. Of note: subsequent experiments were therefore conducted in female and male, 20–35-week-old mice. Flow cytometry evaluation of circulating B cells revealed that APP/PS1 mice also markedly upregulated B cells expressing IL10 (Fig. 2C) as in 3 $\times$ TgAD mice (Fig. 1F). However, APP/PS1 mice did not upregulate 4-1BBL<sup>+</sup> B cells (presumably due to their relatively young age<sup>22,23</sup>) despite a significant increase of B1a cells in circulation and the cLN compared with control littermates (Supplementary Fig. 2B, C). We next generated B-cell-deficient APP/PS1-BKO mice by crossing APP/PS1 and J<sub>H</sub>T mice. Analysis of spatial learning using the MWM revealed that compared with age- and sex-matched APP/PS1 or WT littermates, B-cell deficiency significantly improved learning deficiency in APP/PS1 mice as evident by latency to reach the escape platform ( $F(2,33) = 8.288$ ,  $p = 0.0012$ ; WT vs APP/PS1  $p = 0.0006$ , APP/PS1 vs APP/PS1-BKO  $p = 0.003$ ,  $n = 12$ , Fig. 2D); and in the number of platform region crossings in a probe test conducted 24 h following learning (Kruskal–Wallis ANOVA  $p = 0.0004$ ; WT vs APP/PS1  $p = 0.0002$ ; APP/PS1 vs APP/PS1-BKO  $p = 0.028$ , Fig. 2E). Consistent with the lack of exploratory behavior impairment in APP/PS1 mice<sup>30</sup>, no difference in exploratory behavior of our mice in the OFA (not depicted). Thus, the spatial learning impairments exhibited by APP/PS1 are B-cell dependent.

Because the memory impairments in EOAD are caused by accumulation of A $\beta$  plaques and hippocampal microgliosis<sup>31</sup>, we

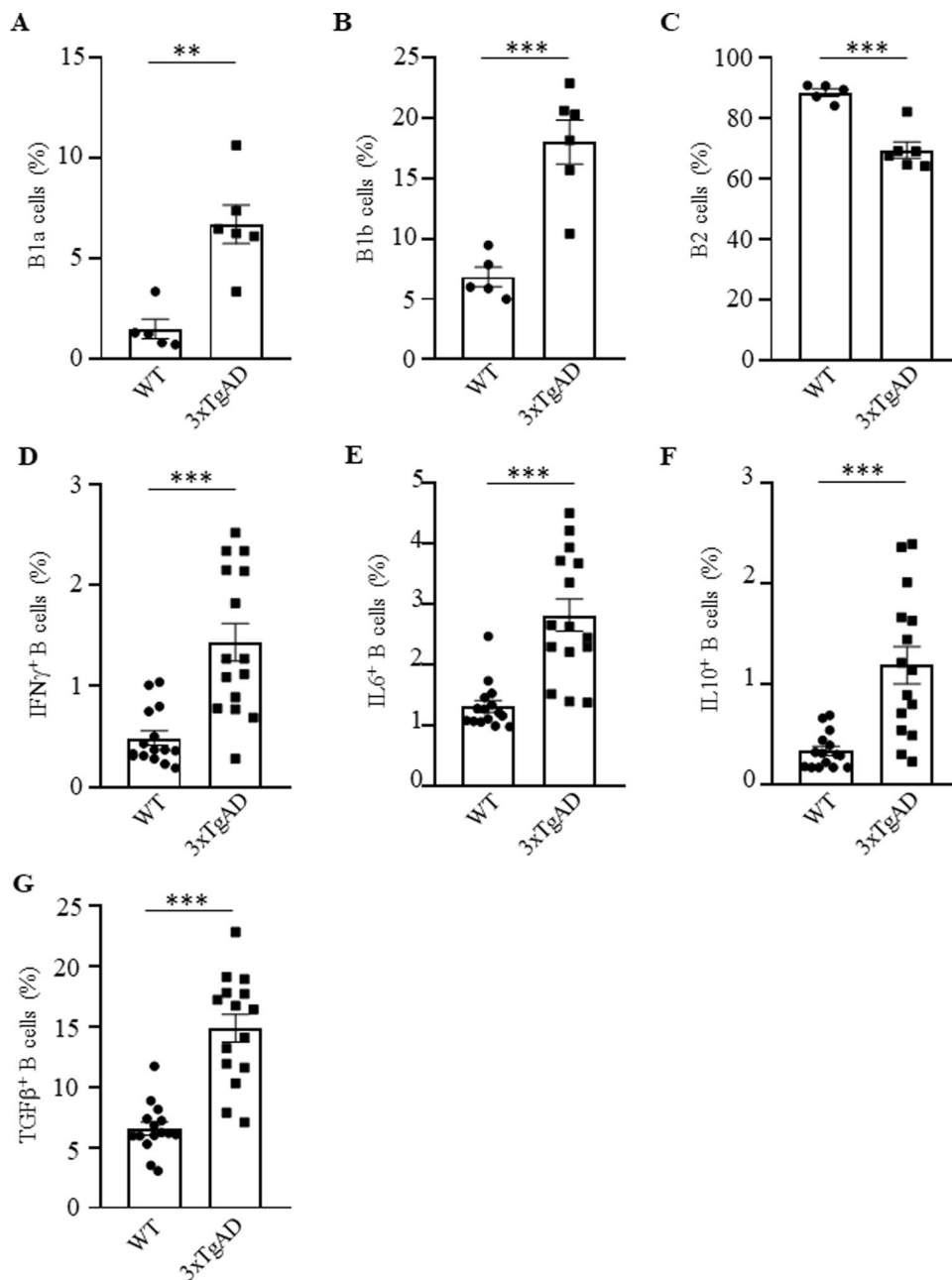


**Fig. 1 Activated B cells were increased in 3xTgAD mice.** Compared with congenic, age- and sex-matched WT mice, B1a (CD5<sup>+</sup>CD11b<sup>+</sup>CD19<sup>+</sup>, **A**) and B1b cells (CD5<sup>+</sup>CD11b<sup>+</sup>CD19<sup>+</sup>, **B**) were increased, while B2 cells (CD5<sup>+</sup>CD11b<sup>-</sup>CD19<sup>+</sup>, **C**) were decreased in the cervical lymph nodes of 3xTgAD mice. AD also activated B cells, as they upregulated IFN $\gamma$  (**D**), IL6 (**E**), IL10 (**F**), and TGF $\beta$  (**G**) in the peripheral blood of mice. Frequency (%) mean  $\pm$  SEM is shown; each symbol is for a single mouse,  $n = 5-6$  in **A-C**,  $n = 15$  in **D-G**. Gating strategy is shown in Supplementary Fig. 9A. \*\* $p < 0.01$ ; \*\*\* $p < 0.001$  in unpaired  $t$  test.

conducted an immunofluorescent analysis for A $\beta$  plaques (using the 6E10 Ab) and ionized calcium binding adaptor 1 (Iba, a microglial cell marker) in cryopreserved brain sections of APP/PS1-BKO (30 weeks old), 3xTgAD-BKO (60–70 weeks old) and age- and sex-matched control mice. Given that in this model the early intraneuronal A $\beta$  deposition in the subiculum is linked to cognitive impairments<sup>32</sup>, and that the subiculum and hippocampal CA1 atrophy is increased in AD patients<sup>33</sup>, from hereon we primarily analyzed the subiculum. It showed a marked upregulation of A $\beta$  plaques in APP/PS1 and 3xTgAD mice (as compared with healthy control mice), which was reversed in APP/PS1-BKO and 3xTgAD-BKO mice respectively ( $n = 4-7$ , Fig. 3A–C and Supplementary Fig. 3A–D). Analysis of frontal

cortex and hippocampus in 3xTgAD-BKO mice also revealed that the increase of soluble A $\beta$ <sub>42</sub> and A $\beta$ <sub>40</sub> was reversed ( $n = 2-6$ , Fig. 3D and Supplementary Fig. 3E). Since both 3xTgAD and 3xTgAD-BKO mice express high levels of the APP transgene in hippocampal neurons (Fig. 3E), we concluded that the benefit of the B-cell deficiency was probably in reduced formation and/or increased clearance of A $\beta$  peptides. Accordingly, large amoeboid microglial cells (>5  $\mu$ m<sup>2</sup>), which indicate dysfunctional overactivation<sup>34,35</sup> and impaired clearance of A $\beta$  plaques<sup>36</sup>, were significantly decreased in 3xTgAD-BKO mice to almost that of in WT mice ( $p < 0.05$ , compared with 3xTgAD,  $n = 3-9$ , Fig. 3F and Supplementary Fig. 3F, G). In contrast, activated microglia (regardless of their size) remained increased in APP/PS1 and

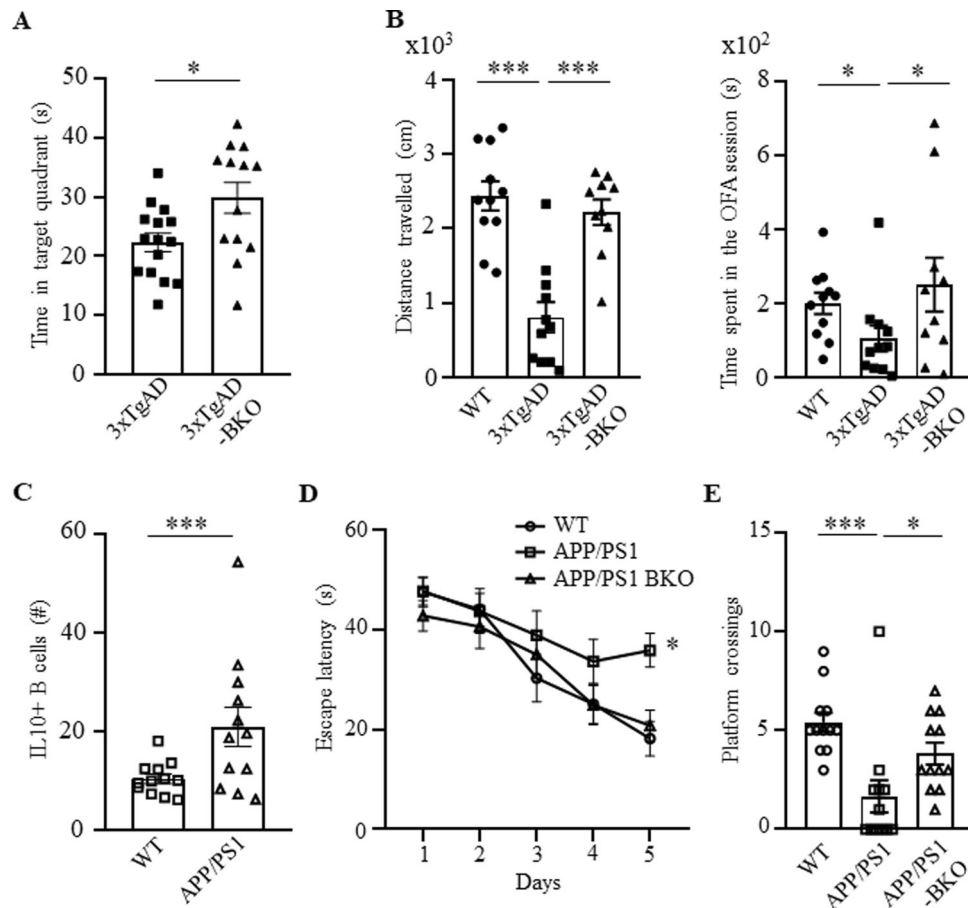


**Fig. 2 Progression of AD required B cells.** The impaired AD-associated cognitive (**A**, the MWM test) and noncognitive locomotion activity (**B**, total distance travelled, left panel, and time spent in center zone, right panel, in 30 min OFA test are shown) of 3×TgAD mice were improved in B-cell-deficient 3×TgAD-BKO mice ( $n = 10\text{--}15$  female). Compared with WT littermate, APP/PS1 mice upregulated numbers of IL10<sup>+</sup> B cells in the peripheral blood (**C**). The impaired cognitive ability of APP/PS1 mice (**D**, latency to reach the escape platform; **E**, platform crossing times in a probe test in MWM test) was reversed in APP/PS1-BKO mice. Mean  $\pm$  SEM is shown; each symbol is for a single mouse. **A**, **B** and **D**, **E** were independently reproduced three and two times, respectively. Gating strategy is shown in Supplementary Fig. 9A. \* $p < 0.05$ ; \*\*\* $p < 0.001$  in unpaired  $t$  test (**A**), Mann-Whitney test (**C**), one-way ANOVA (**B**, left), Kruskal-Wallis test (**B**, right and **E**) or two-way ANOVA (**D**).

APP/PS1-BKO mice (Fig. 3G and Supplementary Fig. 3H). To understand this discrepancy, we compared the function of microglia in these two models. Brain myeloid cells were isolated and stimulated with phorbol 12-myristate 13-acetate and ionomycin (PMAi, which induces microglial cytokine expression and proliferation<sup>37</sup>) for 4–6 h in the presence of monensin, and then surface markers and intracellular (IC) cytokines of microglia (CD45<sup>Int</sup>CD11b<sup>+</sup>) were analyzed using flow cytometry. The loss of B cells did not affect interleukin (IL)1 $\beta$  expression, which was markedly upregulated in both 3×TgAD and APP/PS1 (Supplementary Fig. 4A and Fig. 4A and not depicted; gating strategy is in Supplementary Fig. 9B). In contrast, we noted a marked decrease in TGF $\beta$ <sup>+</sup> and IFN $\gamma$ <sup>+</sup> microglia (presumably quiescent and resting microglia<sup>38–40</sup>) in APP/PS1 and 3×TgAD mice (Fig. 4B, C and Supplementary Fig. 4B–D). The TGF $\beta$ <sup>+</sup> (at lesser extent IFN $\gamma$ <sup>+</sup>) microglial cells were normalized to the levels of WT control in APP/PS1-KO and 3×TgAD-KO mice (Fig. 4B, C and Supplementary Fig. 4B–D). Brain and hippocampal RNA microarray analyses indicated that B-cell deficiency prevented loss of TGF $\beta$ 1<sup>+</sup> microglia in the hippocampi and brains of 3×TgAD mice, as its expression was upregulated (Fig. 4D) while DAM-related transcriptional signature genes, such as *Itgax*, *Cst7*, *Clec7a*, *Mamdc2*, and *Saa3* (ref. 4) were downregulated in 3×TgAD-BKO mice (Supplementary Fig. 4E, Supplementary

Data 1–3, and <https://www.ncbi.nlm.nih.gov/geo/query/acc.cgi?acc=GSE165111>). B-cell deficiency did not affect expression of *IL1 $\beta$*  nor other DAM genes, such as *TNFA*, *Igf1*, and *Lilrb4* (Supplementary Fig. 4E and Supplementary Data 1–3). In sum, despite expression of AD-promoting transgenes, DAM accumulation, A $\beta$  plaque deposition, and thus the disease progression required B cells in both 3×TgAD and APP/PS1 models of AD.

Next, we sought to test whether progression of EOAD can also be controlled by a therapeutic inactivation or depletion of B cells at the disease onset. To test this idea, 3×TgAD mice (60–70 weeks old, female) were intraperitoneally injected with anti-CD20/B220 antibody (which depletes B cells in the circulation) for 2 months. Control mice were treated with isotype-matched IgG. The anti-CD20/B220 Ab efficiently depleted B cells in the circulation (Supplementary Fig. 5A). Compared with control treated mice, the anti-CD20/B220 Ab-treated 3×TgAD showed a trend toward increased activity in the OFA ( $p = 0.07$ , 30 min,  $n = 5$ , Supplementary Fig. 5B). The treatment however significantly reduced the number of A $\beta$  plaques in the subiculum of AD mice ( $p < 0.05$ , Fig. 4E, F), but did not affect the number of large (>50  $\mu\text{m}^2$ ) Iba1<sup>+</sup> microglial cells in the hippocampus (Supplementary Fig. 5C). To understand this discrepancy, we repeated anti-CD20/B220 Ab treatment in a different cohort of female 60–70-week-old 3×TgAD mice for 2 months ( $n = 6\text{--}7$ ) and then performed a flow cytometry

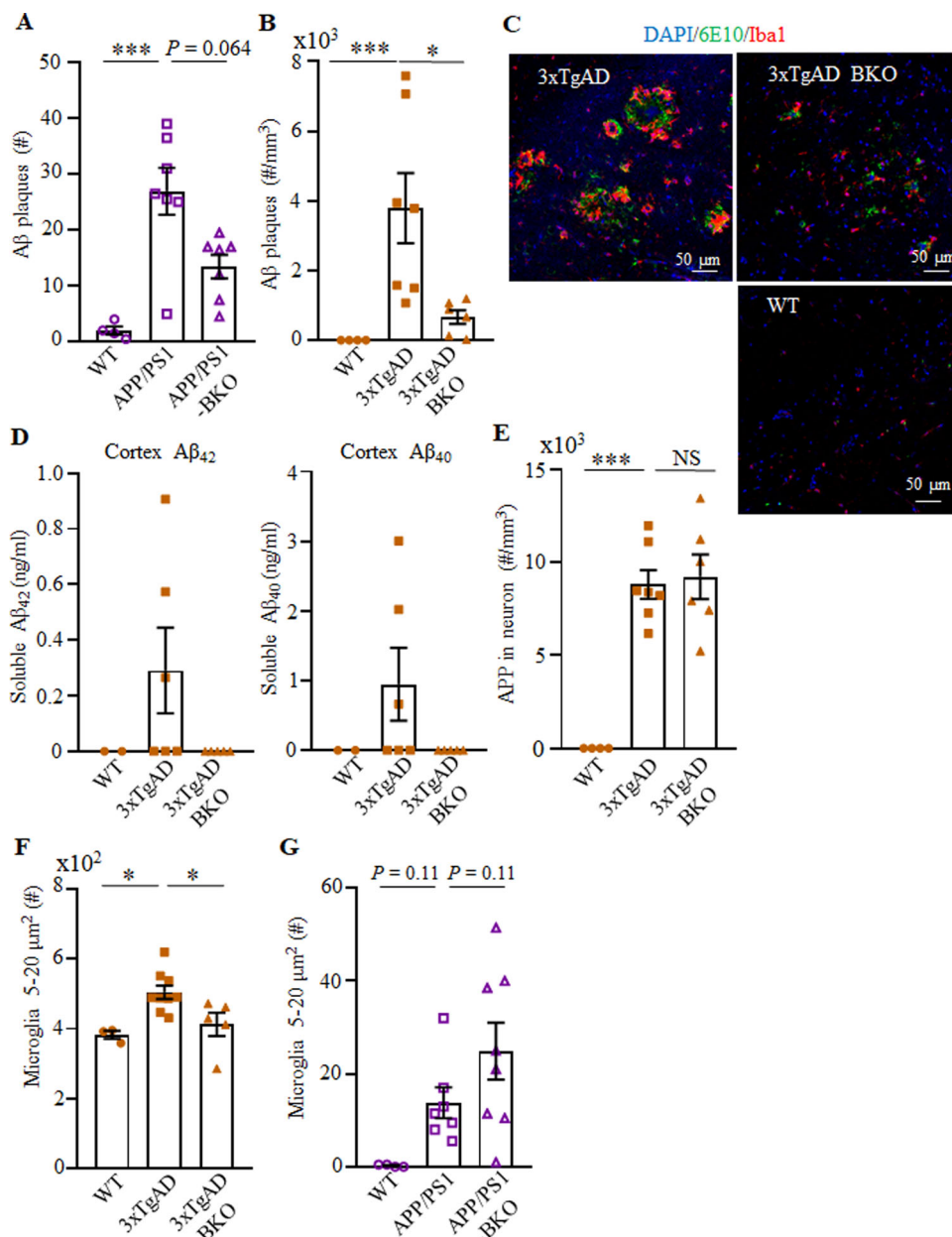


**Fig. 3 B-cell deficiency reduced the Aβ plaque burden and microglial activation in the hippocampus of AD mice.** **A–C** show the number of Aβ plaques in APP/PS1 (**A**) and 3×TgAD (**B**) mice ( $n = 4–7$ ), and representative images of immune fluorescent staining of the subiculum of WT, 3×TgAD, and 3×TgAD-BKO mice (**C**, Aβ plaque (green), Iba1<sup>+</sup> microglia (red), and DAPI (blue); scale, 50 μm). **D** The increase of soluble Aβ<sub>1–40</sub> and Aβ<sub>1–42</sub> peptides in the brain of 3×TgAD mice was reversed in 3×TgAD-BKO mice. The results of ELISA in the cortex of indicated mice ( $n = 2–6$ ) are shown. The B-cell deficiency did not affect expression of the transgene, as both 3×TgAD and 3×TgAD-BKO highly expressed transgenic hAPP in hippocampal neurons (**E**, stained with 6E10 as in **B–C**). The B-cell deficiency significantly decreased the number (#) of large-sized microglia (5–20 μm<sup>2</sup>) in 3×TgAD ( $n = 3–9$ , **F**), but not in APP/PS1 mice ( $n = 4–8$ , **G**). Mean ± SEM is shown; each symbol is for a single mouse. \* $p < 0.05$ ; \*\*\* $p < 0.001$ ; NS not significant in Kruskal-Wallis test (**A**, **B**, **G**) or one-way ANOVA (**E**, **F**).

evaluation of microglial cytokines in the perfused brains. As noted above, in 3×TgAD-BKO mice, B-cell depletion significantly reversed the decrease of TGFβ<sup>+</sup> and IFNγ<sup>+</sup> microglia in 3×TgAD mice to almost the levels in WT mice (both in terms of frequency and numbers,  $p < 0.05$ , Fig. 4C, G and Supplementary Fig. 5D, E) while not affecting IL1β<sup>+</sup> microglia, which was comparably upregulated in aged 3×TgAD and WT mice (Supplementary Fig. 5F).

To validate these results, we used a third mouse model of EOAD, the 5×FAD mice that develop a more aggressive AD pathology by 40 weeks of age because of a large burden of Aβ

plaques caused by additive effects of five familial AD mutations<sup>41</sup>. In this model, others have linked AD progression to a decrease in frequency of potentially beneficial B1a cells<sup>42</sup>. However, our cohorts of 5×FAD mice did not exhibit a decrease in B cells, including B1a and B1b cells (both in terms of number and frequency), as compared with control age-matched littermates (Supplementary Fig. 6A, B). The B cells and B1 cells in 5×FAD mice instead appeared to be activated, as they significantly upregulated expression of 4-1BBL (Supplementary Fig. 6C, D). In concordance, IC cytokine staining of splenic cells revealed marked increase of IL10, TGFβ, and IFNγ in B cells

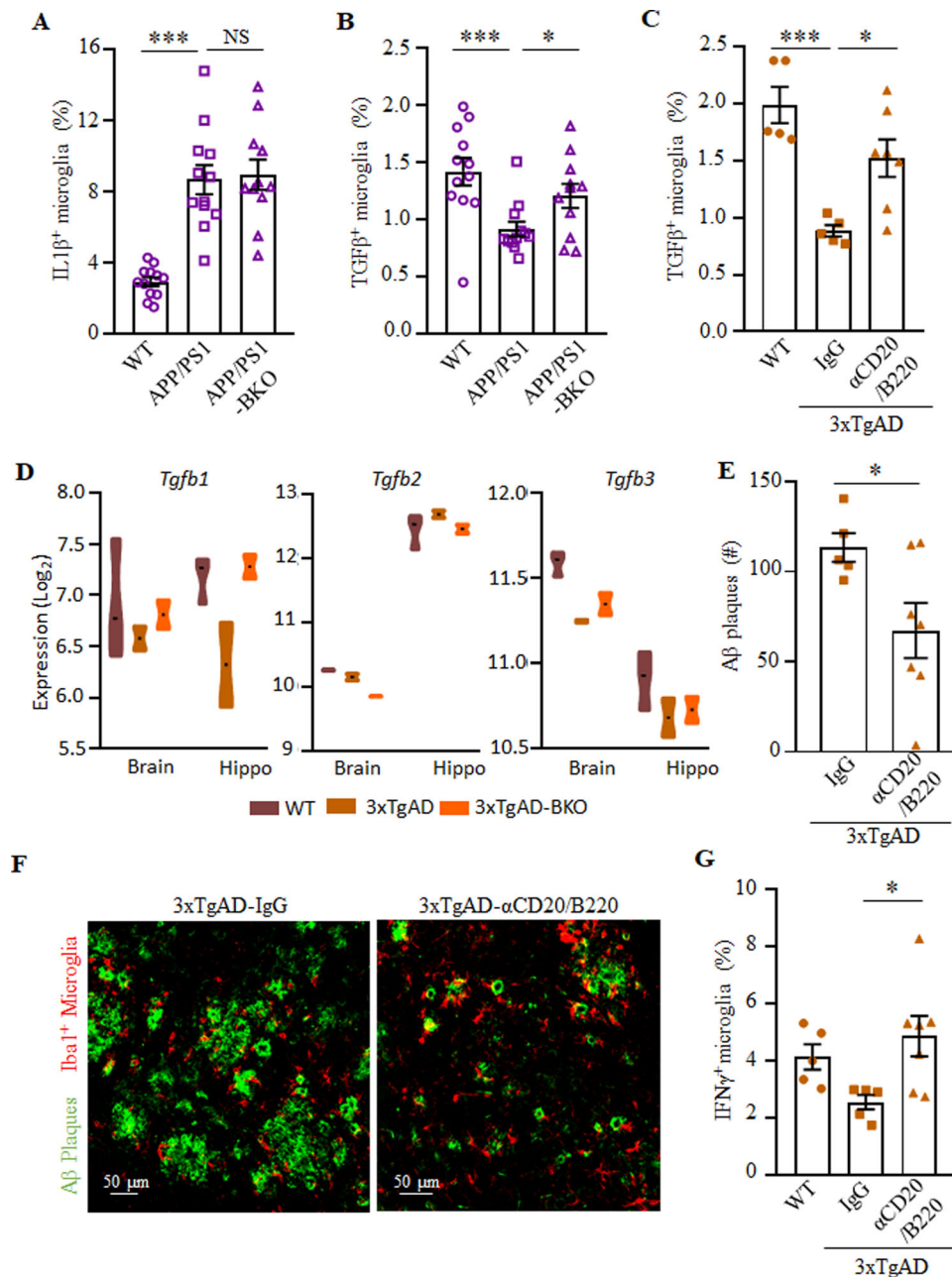


**Fig. 4 B-cell deficiency at least in part reversed the DAM phenotype.** The results of flow cytometric quantification of IL1 $\beta$ <sup>+</sup> (**A**) and TGF $\beta$ <sup>+</sup> (**B**, **C**) microglia (CD11b<sup>+</sup>CD45<sup>int</sup>) in the brains of indicated mice ( $n = 11$ – $12$ ) are shown. Genetic B-cell deficiency in APP/PS1 mice (APP/PS1-BKO, **B**) or transient depletion of circulating B cells ( $\alpha$ CD20/ $\beta$ 220, **C**) at the onset of AD (70–79 weeks of age 3xTgAD mice) reversed the AD-associated decrease of TGF $\beta$ <sup>+</sup> microglia. mRNA microarray analyses of hippocampi and brains (without hippocampus) of 3xTgAD mice revealed that the B-cell deficiency (3xTgAD-BKO) upregulates expression of TGF $\beta$ 1, but not TGF $\beta$ 2 and TGF $\beta$ 3 (**D**,  $n = 3$ ). Therapeutic depletion of B cells ( $\alpha$ CD20/ $\beta$ 220) at the onset of AD ameliorated AD (**E**–**G**), as it markedly decreased A $\beta$  plaques in the subiculum (quantification and representative images are shown in **E** and **F**, respectively; A $\beta$  plaque (green) and Iba1<sup>+</sup> microglia (red, **F**),  $n = 6$ – $8$ ; independently reproduced twice). B-cell depletion reversed the reduction of IFN $\gamma$ <sup>+</sup> microglia in 3xTgAD mice (**G**,  $n = 5$ – $7$ ). Mean  $\pm$  SEM is shown; each symbol is for a single mouse. Gating strategy is shown in Supplementary Fig. 9B. \* $p < 0.05$ ; \*\*\* $p < 0.001$  in one-way ANOVA (**A**–**C**, **G**) or unpaired  $t$  test (**F**).

(Supplementary Fig. 6E). To test whether depletion of these activated B cells also ameliorates AD, 5xTgAD mice (35–47 weeks old, female) were i.p. injected with anti-CD20/ $\beta$ 220 Ab or control IgG ( $n = 7$ – $12$ ) for 2 months. Mice were then evaluated in the OFA for exploratory behavior and anxiety. While control IgG-treated 5xTgAD mice showed reduced exploratory behavior compared with WT littermates, this effect was reversed in B-cell-depleted mice ( $F(2,25) = 5.25$ ,  $p = 0.013$ ; wt vs 5xTgAD  $p = 0.03$ , 5xTgAD+IgG vs 5xTgAD +  $\alpha$ CD20  $p = 0.02$ , Fig. 5A). To confirm

this result, we quantified A $\beta$  plaques and activated microglia in the hippocampus of these mice. Compared with IgG treatment, B-cell depletion in 5xTgAD mice significantly reduced the number of A $\beta$  plaques (Fig. 5B, C) and the large-sized Iba1<sup>+</sup> microglia (Fig. 5D). We repeated the 2-month B-cell depletion experiment in a different cohort of age-matched, female 5xTgAD and WT mice ( $n = 5$ – $12$ ), and evaluated microglial cells using flow cytometry in perfused with saline brains. Similar to 3xTgAD and APP/PS1 mice, TGF $\beta$ <sup>+</sup> and IL10<sup>+</sup> microglia were significantly

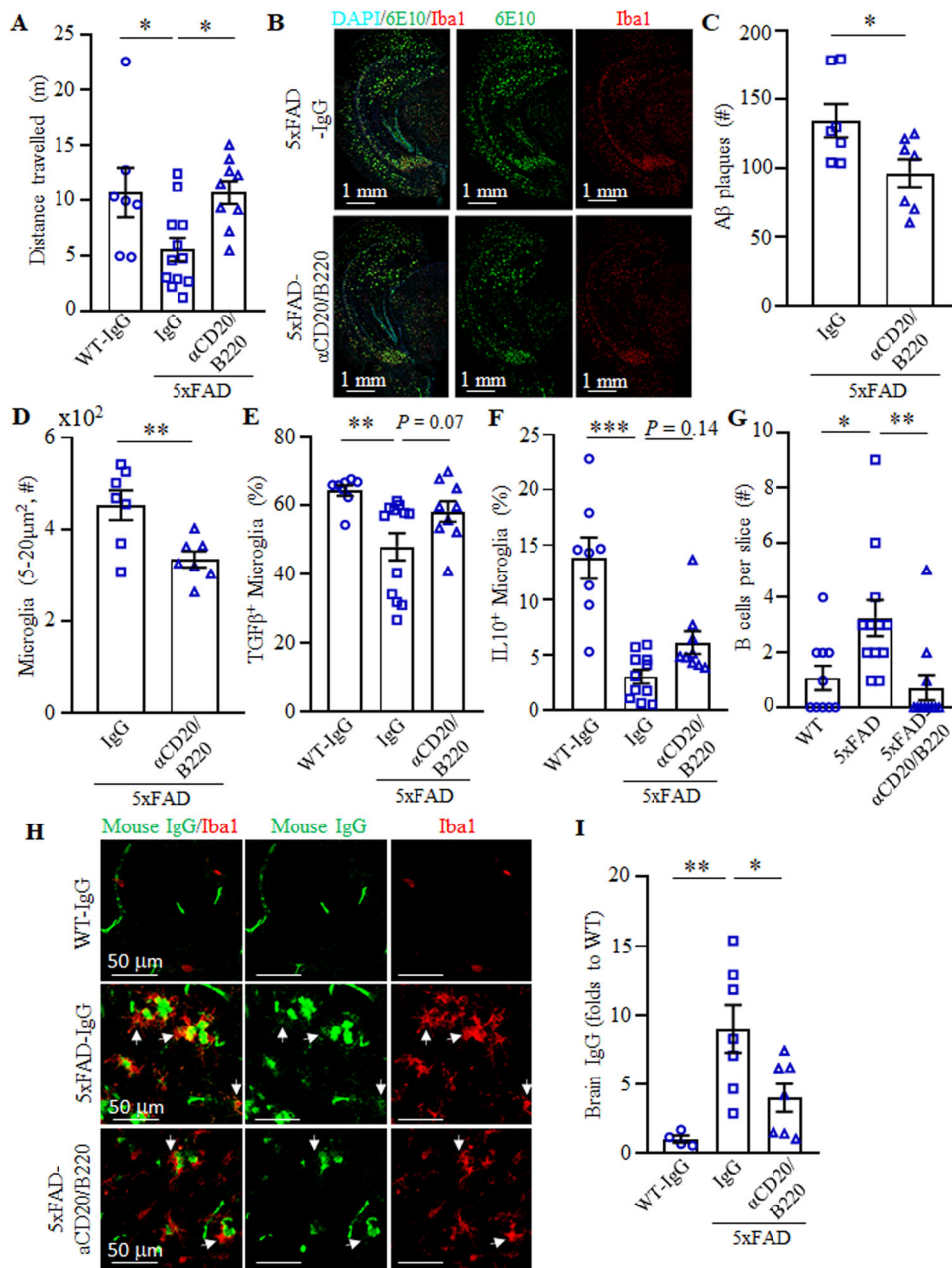


**Fig. 5 Therapeutic depletion of B cells improves AD symptoms in 5x FAD mice.** OFA test revealed that B-cell depletion improves the retarded locomotion of 5x FAD mice (**A**, total distance travelled in first 5 min). B-cell depletion reduced Aβ plaque burden in the hippocampus (**B**, **C**). Representative immune fluorescent staining images for Aβ plaques (green), Iba1<sup>+</sup> microglia (red), and DAPI (cyan) are shown in **B**. In **C** and **D**, the results of quantification of Aβ plaques and microglia are shown (**D**, large size, 5–20 μm<sup>2</sup>), respectively. **A–D** Results were reproduced twice, *n* = 7–12. Flow cytometric evaluation of brain microglia (CD11b<sup>+</sup>CD45<sup>int</sup>) revealed that B-cell depletion increases the frequency (%) of TGFβ<sup>+</sup> (**E**) and IL10<sup>+</sup> (**F**) microglia in 5x FAD mice (*n* = 10–12). As shown with immune fluorescent staining, B220<sup>+</sup> B cells were markedly increased in the brain parenchyma of 5x FAD compared with WT controls, which was lost after transient B-cell depletion (**G**, *n* = 9–12). The brains of 5x FAD mice contained high levels of IgG as compared with WT controls, which was also reversed by transient depletion of B cells (**H** and **I**). In **H**, IgG is green and Iba1<sup>+</sup> microglia is red. Brain IgG quantification is in **I** (*n* = 5–7). Mean ± SEM is shown; each symbol is for a single mouse. Gating strategy is shown in Supplementary Fig. 9B. \**p* < 0.05; \*\**p* < 0.01; \*\*\**p* < 0.001 in one-way ANOVA (**A**, **E**, **F**, **I**), Kruskal-Wallis test (**G**), or unpaired *t* test (**C**, **D**).

decreased in 5x FAD mouse brains as compared with that of WT mice (*p* < 0.001, Fig. 5E, F). B-cell depletion reversed the decrease of TGFβ<sup>+</sup> and IL10<sup>+</sup> microglia in 5x FAD mice (Fig. 5E, F). As in other models, the treatment did not decrease hippocampal IL1β<sup>+</sup> microglia (Supplementary Fig. 7A, B), presumably to support clearance of Aβ plaques<sup>43</sup>. Collectively, we concluded that depletion of B cells can retard progression of AD even if applied at the onset of the disease.

We then wondered whether B cells promote AD by infiltrating the brain parenchyma. Since the low numbers of B cells (<1% of CD45<sup>+</sup> cells, not depicted) detected in flow cytometric analyses cannot discriminate between cells residing inside or outside of the parenchyma, we performed immune fluorescent staining of perfused and cryopreserved brain sections of mice. Unlike control age-matched WT mouse brains, we clearly detected a significant increase of B cells in the parenchyma of frontal cortex and



hippocampus of 5×FAD mice (Fig. 5G and Supplementary Fig. 7C–E). Importantly, this increase of B cells was almost completely lost in B-cell-depleted 5×FAD mice (Fig. 5G and Supplementary Fig. 7D, E), implying that the cells originated in the circulation. We also stained the brain sections for the presence of IgG. While WT mouse brains were almost devoid of immunoglobulin (Fig. 5H, I), readily detectable and numerous IgG foci were present in the hippocampus parenchyma of 5×FAD mice often colocalized with microglia and A $\beta$  plaques (Fig. 5H, I). This brain IgG increase was lost in B-cell-depleted 5×FAD mice (Fig. 5H, I). However, the depletion did not affect levels of total IgG nor minuscule amounts of A $\beta$ -specific antibody in the circulation (Supplementary Fig. 8A–C), implying that B cells in the brain parenchyma produced IgG and presumably promoted AD.

## Discussions

Taken together, we provide counterintuitive evidence for a “dark” side of B cells—they exacerbate manifestation of AD-like symptoms in addition to producing potentially beneficial A $\beta$  plaque-reducing immunoglobulins<sup>17–21</sup> and expressing AD-ameliorating cytokines<sup>42</sup>. Although the exacerbation in Rag-deficient APP and 5×FAD mice is linked to the loss of protective B cells and T cells<sup>16,21</sup>, our data revealed that the genetic loss of B cells alone or their transient depletion at the onset of AD improves the disease symptoms of three different mouse models. Unlike a recent report that linked AD progression to the reduction of anti-inflammatory B1a cells in 5×FAD mice<sup>42</sup>, the numbers of B1a and B1b cells in PB, spleen, and cLN were either unaffected (in 5×FAD mice even when followed for 4, 7, and 12 months) or upregulated (in 3×TgAD and APP/PS1 mice). However, regardless of their numbers, we recently reported that the function of B1a cells is not static and is rather controlled by the inflammatory milieu. In the aged hosts, B1a cells lose their anti-inflammatory activity and acquire pathogenic functions, such as becoming 4-1BBL<sup>+</sup> B1a cells (termed 4BL cells) that induce cytolytic granzyme-B<sup>+</sup> CD8<sup>+</sup> T cells and promote insulin resistance<sup>23,44</sup>. In concordance, B1 cells (as well B2 cells, in some models) in AD mice also appeared to acquire an inflamed phenotype, as they upregulated expression of cytokines, such as IFN $\gamma$ , IL6, TNF $\alpha$ , and IL10, and/or upregulated TGF $\beta$  and 4-1BBL. Although age-associated B cells (CD21<sup>-</sup> CD23<sup>-</sup> CD19<sup>+</sup>) also accumulate in aging, we did not detect their involvement in our three types of mice with AD.

Consistent with a recent RNA-seq report that revealed presence of mature B cells in the brains of AD mice<sup>4</sup>, our data indicate that AD increases B cells in the brain, and their IgG in the cortex and hippocampus parenchyma, which was often colocalized with A $\beta$  plaques and activated microglia. As in multiple sclerosis and cognitive dysfunction following stroke<sup>45–47</sup>, B cells in the brain presumably produce immunoglobulins and proinflammatory factors exacerbating AD-promoting neuroinflammation. First, transfer of IgG from the circulation into the brain is an inefficient process, as only 0.0017% of intravenously injected immunoglobulin reaches the hippocampus of WT and AD mice<sup>48</sup>. Second, consistent with presumed ability of the intra-blood-brain-barrier sites of AD patients to synthesize immunoglobulin<sup>49</sup>, transient depletion of B cells in 5×FAD mice significantly decreased brain B cells and IgG without affecting A $\beta$ -specific and nonspecific antibody levels in sera. Although immunoglobulin is thought to activate and promote microglial uptake of A $\beta$  plaques<sup>21</sup>, the A $\beta$ -IgG complex in CSF is thought to negatively affect the cognitive status of AD patients<sup>50</sup>. Our data also indicate that the loss of B cells, thus IgG, in the brain significantly retards the development of AD. Although the mechanism of this process is a topic of a different study, we think

that brain IgG (or its immune complex) alone or in concert with B-cell cytokines exacerbates neuroinflammation in AD. To do this, the brain IgG presumably targets chronically stressed DAMs (and other brain cells)<sup>4</sup> through their upregulated Fc-receptors and complement<sup>51–53</sup>, as recently shown for myelin-IgG immune complexes from the brain of people with multiple sclerosis, which break immune tolerance of human microglia to microbial stimuli and cause harmful neuroinflammation via Fc $\gamma$ RI and Fc $\gamma$ RIIa<sup>54</sup>. This in turn leads to downregulation of TGF $\beta$ <sup>+</sup> microglia, i.e., reduction in survival of resting M0 microglia and A $\beta$  plaque clearance<sup>3,40,55</sup>. Similar decrease in expression of TGF $\beta$  in DAM and increase in signals of mature B cells is also noted in recent brain RNA-seq results of AD mice<sup>4</sup>. Conversely, the loss of B cells increased TGF $\beta$ <sup>+</sup> microglia as well downregulated expression of *Trem2*, *Clec7a*, and *Itgax* in the hippocampus, i.e., replacement of DAM with microglia that eliminate A $\beta$  oligomers and other neurotoxic debris<sup>8–10</sup>, reduced A $\beta$  plaques and improved behavioral impairments of our AD mice. It is tempting to speculate that B cells similarly participate in EOAD in humans, as the severity of the disease in humans with mild AD is correlated with accumulation of double negative memory CCR6<sup>+</sup> B cells in the circulation<sup>56</sup>. Moreover, elderly humans accumulate pathogenic 4-1BBL<sup>+</sup>TNF $\alpha$ <sup>+</sup> B cells that induce antigen-specific CD8<sup>+</sup> T cells and promote insulin resistance<sup>22,23</sup>, two events linked to AD<sup>57,58</sup>. We therefore propose that the inactivation of B cells can also benefit humans with AD, as therapeutic B-cell removal even at the onset of the disease reversed manifestation of AD in mice.

## Methods

**Mouse.** The animal protocols were approved and permission was granted to perform animal experiments by the ACUC committee of the National Institute on Aging (ASP 321-LMBI-2022) under the Guide for the Care and Use of Laboratory Animals (NIH Publication No. 86-23, 1985). AD transgenic mice (5–80 weeks of age, females) were bred, aged, and housed in the same, specific pathogen-free environment at the National Institute on Aging (NIA). Female C57BL/6j mice (Stock # 000664) were purchased from Jackson Laboratory (Bar Harbor, ME) and congenic 3×TgAD mice (triple transgenic with three human genes associated with familial AD, B6;129-Psen1<sup>tm1Mpm</sup> Tg(APPswe,tauP301L)1 Lfa/Mmjax)<sup>24,25</sup>, APP/PS1 mice (B6.Cg-Tg(APPswe,PSEN1DE9) 85Dbo/J)<sup>16</sup>, 5×FAD mice expressing mutant human APP and PSEN1 genes (B6.Cg-Tg;APPsweF10n,PSEN1\*<sup>M146L</sup>\*<sup>L286V</sup>)<sup>21</sup> and J<sub>H</sub>T mice (B6.129P2-*Igh-<sup>J</sup>m1Cgn*/J), which do not develop functional B cells in the circulation due to the immunoglobulin J<sub>H</sub> locus deletion<sup>26</sup>, were bred and maintained at NIA, Baltimore, MD. Transient B-cell depletion was performed as previously reported<sup>22,59</sup>, such as mice were injected intraperitoneally (i.p., three to six times for 2–3 months) with anti-CD20 Ab (clone 5D2, Genetech, 100  $\mu$ g/mouse) and anti-B220 Ab (150  $\mu$ g/mouse, TIB-146, BioXCell).

**Tissues and blood processing.** Single-cell suspension of spleen and cLN was prepared using a 70  $\mu$ m cell strainer (BD Falcon, Bedford, MA). Blood was collected in tube with 2 mg/ml of Na-heparin (Sigma). Spleen and blood cell suspensions were treated with ACK buffer to remove red blood cells. The brains were dissociated with Adult Brain Dissociation kit for mouse and rat (MiltenyiBiotec, Auburn, CA) using GentleMACS™ Dissociator (MiltenyiBiotec), following the manufacturer's instruction.

**Flow cytometry (FACS).** Antibodies (Ab, see Supplementary Data 4) to mouse CD19, CD5, CD11b, CD43, 4-1BBL, IFN $\gamma$ , IL1 $\beta$ , TGF $\beta$ , IL10, IL6, CD11b, and CD45 and their isotype-matched control Ab were purchased from Biologend, eBioscience, BD Bioscience, and R&D Systems, unless specified. For IC cytokine staining, cells were stimulated with 50 ng/ml PMA (Tocris Bioscience) and 500 ng/ml ionomycin (Tocris Bioscience) for 1–2 h, followed by Golgi stop for 3–4 h using 10  $\mu$ mol/l of Monensin or Brefeldin A (eBioscience); and then stained following manufacturer's instruction for IC fixation and permeabilization (eBioscience). Concentration of antibody used in FACS staining was 1  $\mu$ g per 10<sup>6</sup> cells. Data were analyzed on FACS Canto II (BD) or CytoFLEX (Beckman Coulter, Inc.) using FlowJo software (Tree Star, Inc.) or CytExpert software (Beckman Coulter, Inc.).

**Brain immune fluorescent staining.** Mice were perfused with PBS for 20–30 min after euthanasia with CO<sub>2</sub>, and the brains were removed and washed with PBS, and then half brain was fixed by 4% PFA in PBS. After 24-h fixation, the brain was transferred to PBS buffer containing 30% sucrose in 15 ml tubes for ~2 days until the brain sank to the bottom. Next, the brains were embedded in OCT compound, frozen on dry ice and stored in –80 °C before cryosection. A total of 30- $\mu$ m thick coronal

sections containing hippocampus were collected with 240  $\mu\text{m}$  interval to get eight sets and two to six slices of each mouse were stained for each immunofluorescence staining. For immunofluorescence staining, we adopted free-floating staining method: after two washes with PBS, the brain slices were incubated in 0.3 M glycine buffer for 30 min at room temperature (RT), and then blocked and permeabilized with IF buffer (2% donkey serum, 2% BSA, and 0.1% Triton X-100 in PBS) for 30–60 min at RT. Brain slices were incubated with designated Abs or their isotype control immunoglobulins purchased from Abcam, overnight at 4 °C followed by 15–60-min incubations at RT. After three washes with PBS, brain slices were incubated with fluorochrome-conjugated secondary Abs from Abcam (Donkey anti-mouse IgG H&L-Alexa Fluor 488; Donkey anti-rabbit IgG H&L-Alexa Fluor 568; Donkey anti-rat IgG H&L-Alexa Fluor 568; Donkey anti-goat IgG H&L-Alexa Fluor 647); at RT for 2 h. After three washes with PBS, slides were mounted with ProLong™ Gold/Diamond Antifade Mountant with DAPI (Invitrogen). For IgG staining, brain slices were incubated with Iba1 antibody for 2 h at RT followed by wash with PBS, and then incubated with Alexa Fluor 488 labeled F(ab')<sub>2</sub>-Goat anti-Mouse IgG (H + L) Antibody (cat # A-11017) and Donkey anti-rabbit IgG H&L-Alexa Fluor 568. The information of the first antibodies used is as below: purified anti- $\beta$ -Amyloid, 1-16 Antibody (clone 6E10, cat # 803002), Recombinant Anti-Iba1 antibody (cat # ab178846), Mouse IL1 beta /IL-1F2 Antibody (cat # AF-401-NA), Anti-CD45R (B220) antibody (cat # ab64100), ZO-1 Polyclonal Antibody (cat # 40-2300), and Mouse Laminin alpha 4 Antibody (cat # AF3837).

Images were acquired with a Zeiss LSM 710 confocal microscope equipped with a  $\times 20/0.8$  and a  $\times 20$  Plan-Apochromat dry objectives (Carl Zeiss). For A $\beta$  plaque and microglia quantification, subiculum region for 3 $\times$ TgAD model, or dentate gyrus region for APP/PS1 model, or whole hippocampus region for 5 $\times$ FAD model were respectively identified in the coronal brain slices and imaged. For brain IL1 $\beta$  or IgG quantification, subiculum region was imaged. For brain B220<sup>+</sup> B-cell quantification, the whole brain was observed and images for B220<sup>+</sup> B cells were captured. The quantification of all images was performed with ImageJ software. For A $\beta$  and microglia quantification, the image of up to six slices per mouse were acquired and quantified in the subiculum region (3 $\times$ TgAD model), DG region (APP/PS1 model), or whole hippocampus (5 $\times$ FAD model). Briefly, the single channel image was converted into 8-bit image and proper threshold was chosen and fixed for all the images in the same experiment, then “analyze particles” function was used for quantified the number or area of 6E10 plaque and Iba1<sup>+</sup> microglia. The representative image for microglia quantification was shown in Supplementary Fig. 3G. For B220<sup>+</sup> B-cell quantification, the whole brain region was carefully observed and the images of B220<sup>+</sup> B cells were acquired, and the location of B cells was distinguished by ZO-1 or laminin a4 staining or bright field.

**Measurement of soluble A $\beta$ <sub>40/42</sub> peptides.** Cerebral cortex and hippocampus were separated from PBS-perfused mouse brains, and stored at –80 °C. Soluble and insoluble protein fractions were purified using a modification of previously published protocol for A $\beta$  peptides<sup>60</sup>. Briefly, tissues were mechanically homogenized in TBS-Triton 1% (120 mM NaCl, 50 mM Tris, pH 8.0, 150 mg/ml (tissue/buffer)), including protease inhibitor cocktail (1:100, P2714, Sigma, St. Louis, MO), then incubated on ice for 30 min followed by centrifugation for 120 min at 17,000  $\times$  g at 4 °C. Supernatant, containing TBS-T-soluble fraction of mouse A $\beta$ <sub>1–40</sub> and A $\beta$ <sub>1–42</sub> was removed and stored at –20 °C. The remaining pellet, containing insoluble A $\beta$  was resuspended in 70% formic acid and incubated on ice for 30 min, followed by centrifugation at the same conditions as mentioned above. Formic acid-soluble supernatant was separated and neutralized using 1 M Tris (pH = 11, 20-time the volume of the formic acid) and stored at –20 °C. Total protein concentration was determined using the BCA method (cat # 23225, Thermo Fisher Scientific, Waltham, MA). TBS-S and formic acid soluble levels A $\beta$ <sub>1–40</sub> and A $\beta$ <sub>1–42</sub> in the cortex were measured using sandwich-ELISA protocol in 96-well polystyrene microplates (655061, Greinerbio-one, Monroe, NC) were covered with 50  $\mu\text{l}$  of anti-rabbit-N-terminus A $\beta$ <sub>1–14</sub> (ab2539, Abcam, Cambridge, UK) at a concentration of 5  $\mu\text{g}/\text{ml}$  in carbonate-bicarbonate buffer (pH = 9.6) and incubated overnight at 4 °C. Plates were washed four times in PBS-T solution (0.1% Triton X in PBS) and blocked with 2% BSA solution in PBS. A total of 50  $\mu\text{l}$  of tissue homogenate were applied to each well, and incubated for 60 min at RT. Plates were then washed five times in PBS-T, and the following detection antibodies were added: Anti-A $\beta$ <sub>1–40</sub> antibody (ab20068, Abcam, Cambridge, UK) diluted at 1:500 or anti A $\beta$ <sub>1–42</sub> antibody (05-831, Millipore, Billerica, MA) at 1:2500, and incubated for 60 min at RT. Next, plates were washed five times in PBS-T and secondary goat anti-mouse IgG HRP-conjugated antibody was added (115-035-003, Peroxidase AffiniPure Goat Anti-Mouse, Jackson immunoresearch, PA) at a dilution of 1:5000. Plates were washed five times with PBS-T and 50  $\mu\text{l}$  of 3, 3', 5, 5'-tetramethylbenzidine substrate (00-4201-56, Affimetrix eBioscience, San Diego, CA) was added. The color reaction was allowed to develop for 3 min and was stopped by adding 50  $\mu\text{l}$  of 2 M H<sub>2</sub>SO<sub>4</sub>. Optical density was measured at 450 nm using a spectrophotometer. Standard curve was carried out using known concentrations of recombinant A $\beta$ <sub>1–40</sub> and A $\beta$ <sub>1–42</sub>.

**Behavioral tests.** For the MWM test, we used a 140-cm-diameter tub containing a 15  $\times$  15 cm square platform submerged 1 cm below the water surface. Water was maintained at 21  $\pm$  1 °C and colored with white paint. Mice underwent four trials per day, released from each of four compass points (N, S, W, E) in a randomized order. If a mouse did not find the hidden platform within 60 s, it was gently guided to the platform. All mice remained on the platform for 10 s at the end of each trial,

were towel dried, and returned to their home cage. After 5 days of training mice were subjected to a 60-s probe trial that took place 24 h after the last training trial. The platform was removed and mice were placed on the opposite wall at the point furthest from the former platform location. The day after the probe trial, mice were tested for four trials in their ability to swim to a visible platform. Swimming was analyzed with ANY-Maze software (Stoelting). For the open field test, mice were placed in a 34  $\times$  34  $\times$  25 cm white acrylic chamber and recorded by overhead camera for 60 min. Because the first few minutes in this test are maximally sensitive to AD transgenic mice<sup>30</sup>, we focused analysis on the initial 5 minutes. Tracks were analyzed with ANY-Maze software. Analysis in all behavior experiments was performed using ANY-Maze software. For the gait analysis, mice were tested on a fixed-speed treadmill apparatus (DigiGait; Mouse Specifics). Mice were habituated to the apparatus for 1 min, and then given a 1-min run at 5 cm/s. Following a 1-min rest, the treadmill speed was increased to 15 cm/s. Video was collected at high speed from a ventrally placed camera, and 3–5 s of representative gait video was selected by an experienced user for automated analysis.

**Microarray analysis.** From PBS-perfused brains or hippocampi of mice, total RNA was isolated with RNeasy Plus micro kit (QIAGEN) according to manufacturer's instruction. Microarray analysis was performed using the Illumina and Agilent platforms, then we quantile-normalized the gene expression profiles<sup>61</sup>, log<sub>2</sub>-transformed the raw probe intensity values and estimated the gene expression using the probe with the highest average expression<sup>62</sup>. Microarray data are submitted at <https://www.ncbi.nlm.nih.gov/geo/query/acc.cgi?acc=GSE165111>.

**Immunoglobulin ELISA.** Blood was collected in BD Microtainer® Tubes and serum was separated by centrifugation following the manufacturer's instruction. For A $\beta$ -specific immunoglobulin ELISA, sera (diluted in 0.05% Tween20/2% BSA/PBS) were incubated in 96-well plates coated with 4–8  $\mu\text{g}/\text{ml}$  A $\beta$ <sub>1–42</sub> peptide (AnaSpec, cat # AS-24224) and quantified using HRP-conjugated goat anti-mouse IgA, IgM, or IgG antibodies. For serum immunoglobulin ELISA, Ig Isotyping Mouse Uncoated ELISA Kit (Invitrogen, Cat No. # 88-50630-88) was used, following the manufacturer's instruction.

**Statistical analysis.** All statistical analyses were performed with GraphPad Prism (Prism 8; Graph Pad Software, Inc.). Normality tests were conducted to decide whether the data are from normally distributed population. Unpaired *t* test or one-way ANOVA, for two groups or three groups, respectively, was used if the data are considered to be normally distributed, otherwise Mann-Whitney test or Kruskal-Wallis test was used for two groups or three groups, respectively. Due to changes in variance across days of invisible platform testing in MWM, as is typical in this task<sup>63</sup>, each day was individually analyzed using one-way ANOVA. Bonferroni post hoc tests were conducted when appropriate. The results were presented as the mean with each individual data point or in bar graph  $\pm$  SEM. A *p* value <0.05 was considered significant (\**p* < 0.05, \*\**p* < 0.01, and \*\*\**p* < 0.001).

**Reporting summary.** Further information on research design is available in the Nature Research Reporting Summary linked to this article.

## Data availability

All data associated with this study can be found in the paper or supplementary materials. The microarray data are deposited at <https://www.ncbi.nlm.nih.gov/geo/query/acc.cgi?acc=GSE165111>. Source data are provided with this paper.

Received: 10 December 2019; Accepted: 12 March 2021;

Published online: 12 April 2021

## References

- Hardy, J. & Selkoe, D. J. The amyloid hypothesis of Alzheimer's disease: progress and problems on the road to therapeutics. *Science* **297**, 353–356 (2002).
- Ma, D. et al. TGF-beta induced by interleukin-34-stimulated microglia regulates microglial proliferation and attenuates oligomeric amyloid beta neurotoxicity. *Neurosci. Lett.* **529**, 86–91 (2012).
- Tichauer, J. E. & von Bernhardi, R. Transforming growth factor-beta stimulates beta amyloid uptake by microglia through Smad3-dependent mechanisms. *J. Neurosci. Res.* **90**, 1970–1980 (2012).
- Keren-Shaul, H. et al. A unique microglia type associated with restricting development of alzheimer's disease. *Cell* **169**, 1276–1290 e1217 (2017).
- Brionne, T. C., Tesseur, I., Masliah, E. & Wyss-Coray, T. Loss of TGF-beta 1 leads to increased neuronal cell death and microgliosis in mouse brain. *Neuron* **40**, 1133–1145 (2003).
- Monje, M. L., Toda, H. & Palmer, T. D. Inflammatory blockade restores adult hippocampal neurogenesis. *Science* **302**, 1760–1765 (2003).

7. Ekdahl, C. T., Claassen, J. H., Bonde, S., Kokaia, Z. & Lindvall, O. Inflammation is detrimental for neurogenesis in adult brain. *Proc. Natl Acad. Sci. USA* **100**, 13632–13637 (2003).
8. Rogers, J., Strohmeier, R., Kovelowski, C. J. & Li, R. Microglia and inflammatory mechanisms in the clearance of amyloid beta peptide. *Glia* **40**, 260–269 (2002).
9. DeWitt, D. A., Perry, G., Cohen, M., Doller, C. & Silver, J. Astrocytes regulate microglial phagocytosis of senile plaque cores of Alzheimer's disease. *Exp. Neurol.* **149**, 329–340 (1998).
10. Mawuenyega, K. G. et al. Decreased clearance of cns beta-amyloid in Alzheimer's disease. *Science* **330**, 1774–1774 (2010).
11. in 't Veld, B. A. et al. Nonsteroidal antiinflammatory drugs and the risk of Alzheimer's disease. *N. Engl. J. Med.* **345**, 1515–1521 (2001).
12. Thevaranjan, N. et al. Age-associated microbial dysbiosis promotes intestinal permeability, systemic inflammation, and macrophage dysfunction. *Cell Host Microbe* **21**, 455–466 e454 (2017).
13. Holmes, C. et al. Systemic infection, interleukin 1beta, and cognitive decline in Alzheimer's disease. *J. Neurol. Neurosurg. Psychiatry* **74**, 788–789 (2003).
14. Fisher, Y., Nemirovsky, A., Baron, R. & Monsonego, A. T cells specifically targeted to amyloid plaques enhance plaque clearance in a mouse model of Alzheimer's disease. *PLoS ONE* **5**, e10830 (2010).
15. Browne, T. C. et al. IFN-gamma production by amyloid beta-specific Th1 cells promotes microglial activation and increases plaque burden in a mouse model of Alzheimer's disease. *J. Immunol.* **190**, 2241–2251 (2013).
16. Spani, C. et al. Reduced beta-amyloid pathology in an APP transgenic mouse model of Alzheimer's disease lacking functional B and T cells. *Acta Neuropathol. Commun.* **3**, 71 (2015).
17. Gold, M., Mengel, D., Roskam, S., Dodel, R. & Bach, J. P. Mechanisms of action of naturally occurring antibodies against beta-amyloid on microglia. *J. Neuroinflammation* **10**, 5 (2013).
18. Britschgi, M. et al. Neuroprotective natural antibodies to assemblies of amyloidogenic peptides decrease with normal aging and advancing Alzheimer's disease. *Proc. Natl Acad. Sci. USA* **106**, 12145–12150 (2009).
19. Morgan, D. et al. A beta peptide vaccination prevents memory loss in an animal model of Alzheimer's disease. *Nature* **408**, 982–985 (2000).
20. Olkhanud, P. B. et al. DNA immunization with HBsAg-based particles expressing a B cell epitope of amyloid beta-peptide attenuates disease progression and prolongs survival in a mouse model of Alzheimer's disease. *Vaccine* **30**, 1650–1658 (2012).
21. Marsh, S. E. et al. The adaptive immune system restrains Alzheimer's disease pathogenesis by modulating microglial function. *Proc. Natl Acad. Sci. USA* **113**, E1316–E1325 (2016).
22. Lee-Chang, C. et al. Accumulation of 4-1BBL+ B cells in the elderly induces the generation of granzyme-B+ CD8+ T cells with potential antitumor activity. *Blood* **191**, 4141–4151 (2014).
23. Bodogai, M. et al. Commensal bacteria contribute to insulin resistance in aging by activating innate B1a cells. *Sci. Transl. Med.* **10**, eaat4271 (2018).
24. Oddo, S. et al. Triple-transgenic model of Alzheimer's disease with plaques and tangles: intracellular Abeta and synaptic dysfunction. *Neuron* **39**, 409–421 (2003).
25. Sterniczuk, R., Antle, M. C., Laferla, F. M. & Dyck, R. H. Characterization of the 3xTg-AD mouse model of Alzheimer's disease: part 2. Behavioral and cognitive changes. *Brain Res.* **1348**, 149–155 (2010).
26. Chen, J. et al. Immunoglobulin gene rearrangement in B cell deficient mice generated by targeted deletion of the JH locus. *Int. Immunol.* **5**, 647–656 (1993).
27. Filali, M. et al. Cognitive and non-cognitive behaviors in the triple transgenic mouse model of Alzheimer's disease expressing mutated APP, PS1, and Mapt (3xTg-AD). *Behav. Brain Res.* **234**, 334–342 (2012).
28. Chiquita, S. et al. A longitudinal multimodal in vivo molecular imaging study of the 3xTg-AD mouse model shows progressive early hippocampal and taurine loss. *Hum. Mol. Genet.* **28**, 2174–2188 (2019).
29. Borchelt, D. R. et al. Accelerated amyloid deposition in the brains of transgenic mice coexpressing mutant presenilin 1 and amyloid precursor proteins. *Neuron* **19**, 939–945 (1997).
30. O'Leary, T. P., Hussin, A. T., Gunn, R. K. & Brown, R. E. Locomotor activity, emotionality, sensorimotor gating, learning and memory in the APPsw/PS1dE9 mouse model of Alzheimer's disease. *Brain Res. Bull.* **140**, 347–354 (2018).
31. Atwood, C. S. & Bowen, R. L. A unified hypothesis of early- and late-onset Alzheimer's disease pathogenesis. *J. Alzheimers Dis.* **47**, 33–47 (2015).
32. Roda, A. R., Esquerda-Canals, G., Marti-Clua, J. & Villegas, S. Cognitive impairment in the 3xTg-AD mouse model of Alzheimer's disease is affected by abeta-immunotherapy and cognitive stimulation. *Pharmaceutics* **12**, 944 (2020).
33. Greene, S. J. & Killiany, R. J., Alzheimer's Disease Neuroimaging, I. Hippocampal subregions are differentially affected in the progression to Alzheimer's disease. *Anat. Rec.* **295**, 132–140 (2012).
34. Stence, N., Waite, M. & Dailey, M. E. Dynamics of microglial activation: a confocal time-lapse analysis in hippocampal slices. *Glia* **33**, 256–266 (2001).
35. Bachstetter, A. D. et al. Disease-related microglia heterogeneity in the hippocampus of Alzheimer's disease, dementia with Lewy bodies, and hippocampal sclerosis of aging. *Acta Neuropathol. Commun.* **3**, 32 (2015).
36. El Hajj, H. et al. Ultrastructural evidence of microglial heterogeneity in Alzheimer's disease amyloid pathology. *J. Neuroinflammation* **16**, 87 (2019).
37. Stebbing, M. J., Cottee, J. M. & Rana, I. The role of ion channels in microglial activation and proliferation - a complex interplay between ligand-gated ion channels, K(+) channels, and intracellular Ca(2+). *Front. Immunol.* **6**, 497 (2015).
38. Abutbul, S. et al. TGF-beta signaling through SMAD2/3 induces the quiescent microglial phenotype within the CNS environment. *Glia* **60**, 1160–1171 (2012).
39. Schilling, T., Nitsch, R., Heinemann, U., Haas, D. & Eder, C. Astrocyte-released cytokines induce ramification and outward K+ channel expression in microglia via distinct signalling pathways. *Eur. J. Neurosci.* **14**, 463–473 (2001).
40. Butovsky, O. et al. Identification of a unique TGF-beta-dependent molecular and functional signature in microglia. *Nat. Neurosci.* **17**, 131–143 (2014).
41. Oakley, H. et al. Intraneuronal beta-amyloid aggregates, neurodegeneration, and neuron loss in transgenic mice with five familial Alzheimer's disease mutations: potential factors in amyloid plaque formation. *J. Neurosci.* **26**, 10129–10140 (2006).
42. Baulch, J. E. et al. Immune and inflammatory determinants underlying Alzheimer's disease pathology. *J. Neuroimmune Pharmacol.* **15**, 852–862 (2020).
43. Shaftel, S. S. et al. Sustained hippocampal IL-1 beta overexpression mediates chronic neuroinflammation and ameliorates Alzheimer plaque pathology. *J. Clin. Investig.* **117**, 1595–1604 (2007).
44. Lee-Chang, C. et al. Aging converts innate B1a cells into potent CD8+ T cell inducers. *J. Immunol.* **196**, 3385–3397 (2016).
45. Michel, L. et al. B cells in the multiple sclerosis central nervous system: trafficking and contribution to CNS-compartmentalized inflammation. *Front. Immunol.* **6**, 636 (2015).
46. Cepok, S. et al. Short-lived plasma blasts are the main B cell effector subset during the course of multiple sclerosis. *Brain* **128**, 1667–1676 (2005).
47. Doyle, K. P. et al. B-lymphocyte-mediated delayed cognitive impairment following stroke. *J. Neurosci.* **35**, 2133–2145 (2015).
48. St-Amour, I. et al. Brain bioavailability of human intravenous immunoglobulin and its transport through the murine blood-brain barrier. *J. Cereb. Blood Flow. Metab.* **33**, 1983–1992 (2013).
49. Blennow, K. et al. Intra-blood-brain-barrier synthesis of immunoglobulins in patients with dementia of the Alzheimer type. *Alzheimer Dis. Assoc. Disord.* **4**, 79–86 (1990).
50. Maffei, M. et al. Increased levels of antigen-bound beta-amyloid autoantibodies in serum and cerebrospinal fluid of Alzheimer's disease patients. *PLoS ONE* **8**, e68996 (2013).
51. Chakrabarty, P. et al. IFN-gamma promotes complement expression and attenuates amyloid plaque deposition in amyloid beta precursor protein transgenic mice. *J. Immunol.* **184**, 5333–5343 (2010).
52. Diamond, B., Huerta, P. T., Mina-Osorio, P., Kowal, C. & Volpe, B. T. Losing your nerves? Maybe it's the antibodies. *Nat. Rev. Immunol.* **9**, 449–456 (2009).
53. Doens, D. & Fernandez, P. L. Microglia receptors and their implications in the response to amyloid beta for Alzheimer's disease pathogenesis. *J. Neuroinflammation* **11**, 48 (2014).
54. van der Poel, M., Hoepel, W., Hamann, J., Huitinga, I. & Dunnen, J. D. IgG immune complexes break immune tolerance of human microglia. *J. Immunol.* **205**, 2511–2518 (2020).
55. Caraci, F. et al. TGF-beta 1 protects against Abeta-neurotoxicity via the phosphatidylinositol-3-kinase pathway. *Neurobiol. Dis.* **30**, 234–242 (2008).
56. Bulati, M. et al. Double negative (IgG+IgD-CD27-) B cells are increased in a cohort of moderate-severe Alzheimer's disease patients and show a pro-inflammatory trafficking receptor phenotype. *J. Alzheimers Dis.* **44**, 1241–1251 (2015).
57. Merlini, M., Kirabali, T., Kulic, L., Nitsch, R. M. & Ferretti, M. T. Extravascular CD3+ T cells in brains of Alzheimer disease patients correlate with tau but not with amyloid pathology: an immunohistochemical study. *Neurodegener. Dis.* **18**, 49–56 (2018).
58. Ferreira, L. S. S., Fernandes, C. S., Vieira, M. N. N. & De Felice, F. G. Insulin resistance in Alzheimer's Disease. *Front. Neurosci.* **12**, 830 (2018).
59. Bodogai, M. et al. Anti-CD20 antibody promotes cancer escape via enrichment of tumor-evoked regulatory B cells expressing low levels of CD20 and CD137L. *Cancer Res.* **73**, 2127–2138 (2013).
60. Illouz, T., Madar, R., Griffioen, K. & Okun, E. A protocol for quantitative analysis of murine and human amyloid-beta1-40 and 1-42. *J. Neurosci. Methods* **291**, 28–35 (2017).

61. Dunning, M. J., Smith, M. L., Ritchie, M. E. & Tavaré, S. beadarray: R classes and methods for Illumina bead-based data. *Bioinformatics* **23**, 2183–2184 (2007).
62. Miller, J. A. et al. Strategies for aggregating gene expression data: the collapseRows R function. *BMC Bioinformatics* **12**, 322 (2011).
63. Vorhees, C. V. & Williams, M. T. Morris water maze: procedures for assessing spatial and related forms of learning and memory. *Nat. Protoc.* **1**, 848–858 (2006).

### Acknowledgements

We are grateful to Dr. A. C. Chan (Genentech, Inc.) for providing anti-CD20 Ab; Drs. K. Becker, E. Lehrmann, and Y. Zhang (NIA) for microarray assay and bioinformatics analysis; and Mrs. A. Lustig (NIA) and Dr. Chandamany Arya (Lilly) for proofreading. This research was supported by the Intramural Research Program of the National Institute on Aging, NIH, and by grant NIH R01 AG054712-01A1.

### Author contributions

K.K., X.W., E.Ra., and M.B. performed the research and collected and analyzed data; T.I., M.D., and R.M. performed experiments; F.G. provided bioinformatics support, E.Ro. and E.O. provided critical interpretation; and A.B. wrote the manuscript and conceived, designed, and supervised the study.

### Funding

Open Access funding provided by the National Institutes of Health (NIH).

### Competing interests

The authors declare no competing interests.

### Additional information

**Supplementary information** The online version contains supplementary material available at <https://doi.org/10.1038/s41467-021-22479-4>.

**Correspondence** and requests for materials should be addressed to A.B.

**Peer review information** *Nature Communications* thanks Jacques Galipeau and the other, anonymous, reviewer(s) for their contribution to the peer review of this work. Peer reviewer reports are available.

**Reprints and permission information** is available at <http://www.nature.com/reprints>

**Publisher's note** Springer Nature remains neutral with regard to jurisdictional claims in published maps and institutional affiliations.



**Open Access** This article is licensed under a Creative Commons Attribution 4.0 International License, which permits use, sharing, adaptation, distribution and reproduction in any medium or format, as long as you give appropriate credit to the original author(s) and the source, provide a link to the Creative Commons license, and indicate if changes were made. The images or other third party material in this article are included in the article's Creative Commons license, unless indicated otherwise in a credit line to the material. If material is not included in the article's Creative Commons license and your intended use is not permitted by statutory regulation or exceeds the permitted use, you will need to obtain permission directly from the copyright holder. To view a copy of this license, visit <http://creativecommons.org/licenses/by/4.0/>.

This is a U.S. government work and not under copyright protection in the US; foreign copyright protection may apply 2021